MEMS Phased Array Detection in Contact with Solids

D.W. Greve and A. Jain
Department of Electrical and Computer Engineering, Carnegie Mellon University, Pittsburgh, PA, USA
I.J. Oppenheim
Department of Civil and Environmental Engineering, Carnegie Mellon University, Pittsburgh, PA, USA

Abstract - We report on the development of transducers for ultrasonic flaw detection which can be permanently mounted at critical locations on structures. We will show that MEMS capacitive diaphragm transducers can be bonded to metal or plexiglas test speciments without damage and that ultrasonic energy can be efficiently coupled into the transducer. It will be demonstrated that transducer arrays can be operated as a phased array in order to determine the direction and distance of an ultrasonic source. In addition, the detection of flaws or voids in a test specimen will also be demonstrated.

I. Introduction

MEMS ultrasonic transducers (sometimes termed cMUTs, for Capacitive MEMS Ultrasonic Transducers), have been studied by several research groups [1,2,3,4]. However to date this previous work concentrated on transducers for air or liquid immersion applications. In this paper, we report on our work with transducers which can be used in direct contact with solids. Such transducers can potentially be used as an economical phased-array detector, permanently bonded to crucial locations in a structure. In conjunction with a single piezoelectric emitter, such an array can detect developing flaws before they cause structural failure.

A crucial issue in this proposed application is the requirement for efficient coupling of ultrasonic energy into the detectors. We will show that efficient coupling can be provided without damaging the detectors, and we will demonstrate successful operation of bonded detector arrays.

II. Transducer Fabrication

The transducer arrays used in this work were fabricated in the MUMPS multi-user MEMS process on 1 cm^2 chips. Each chip contained an array of 9 detectors arranged along one edge spaced 0.99 mm center-to-center. The detectors each consisted of 180 individual capacitive diaphragms. A cross section and top view of the diaphragm design is presented in Fig. 1. The diaphragm is formed between the POLY0 and POLY1 layers; the diaphragm thickness is 2 μm and the electrode gap is also 2 μm. The diaphragms were released by etching a sacrificial oxide through 5 μm square holes.

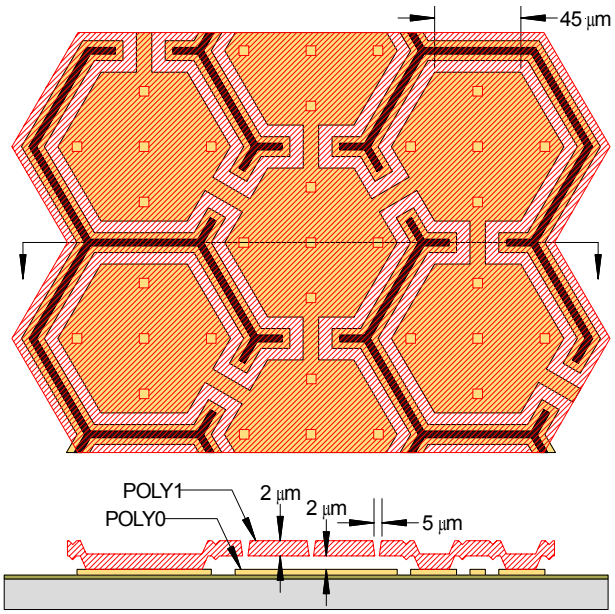

Figure 1. Diaphragm detail.

Detectors were characterized before bonding using admittance-voltage and admittance-frequency measurements using HP 4280A and HP4192A instruments, respectively. Then detectors were bonded to plexiglas or metal specimens using brush-applied silicone (Gelest Zipcone CG) as an adhesive.

III. Transducer Characterization

Figure 2 shows the measured admittance of an unbonded transducer as a function of frequency for four different pressure conditions. The transducer exhibits a resonance near 3.47 MHz, which is in reasonable agreement with calculations based on the transducer dimensions [5]. When operated at atmospheric pressure the diaphragm is damped by squeeze-film damping associated with the etch holes and also radiation of acoustic energy. In contrast, measurements under vacuum conditions reflect the internal damping of the diaphragm itself. From these measurements, it is possible to extract the acoustic impedance of the dia-

phragm, including the radiation and squeeze-film damping terms.

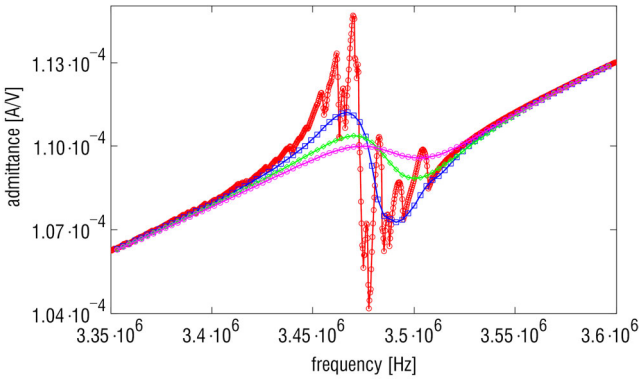

Figure 2. Measured admittance magnitude |Y(ω)| as a function of pressure: (○) coarse vacuum; (□) 0.29 atm; (◇) 0.61 atm; (+) 1 atm (all with V_{DC} = 35 V) and (—) coarse vacuum, V_{DC} = 0 V.

Details of the the diaphragm modeling are available elsewhere [5]. We are concerned with the diaphragm acoustic impedance in the range of frequencies of interest for ultrasonic flaw detection (roughly 1 MHz-10 MHz). The diaphragm acoustic impedance is considerably lower (1-2 orders of magnitude) than that of silicone or the solid materials over this entire range of frequencies. To a good approximation, then, the coupled transducer can be approximated by a short circuit.

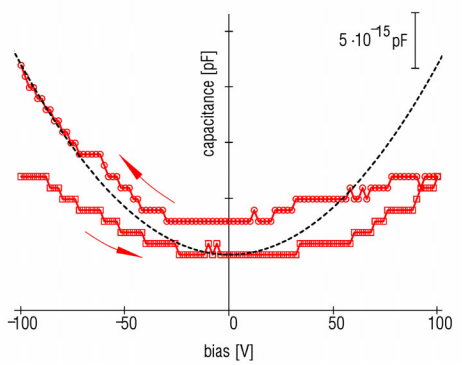

Figure 3. 1 MHz capacitance-voltage measurements for a bonded transducer (points) and for unbonded transducer (dashed line).

We can demonstrate that the transducer is coupled to the solid by comparing C(V) measurements before and after bonding. These measurements are shown in Fig. 3. The measurement frequency is 1 MHz which is far from the resonant frequency and consequently the capacitance change is due to the diaphragm deflection caused by the DC bias. For an unbonded diaphram we expect $C(V) = C_0 + C_1 V^2$ where C_0 is the capacitance of the diaphragm with no applied DC bias and C_1 is proportional to the diaphragm flexibility. The dashed line in Fig. 3 shows the measured capacitance for an unbonded diaphragm. For a bonded diaphragm (squares) the capacitance change is reduced compared to the unbonded case and hysteresis is observed. This is consistent with bonding of the diaphragm to a flexible medium.

IV. Acoustic Coupling

Figure 4 shows schematically the diaphragm coupled to a solid specimen with a thin layer of silicone. The thickness of the adhesive silicone layer has been measured and is approximately 20 μm, considerably less than an acoustic wavelength (370 μm at 3.5 MHz). The effectiveness of acoustic coupling can be predicted using a transmission line model (Fig. 4, bottom). The free surface of a solid with acoustic impedance Z_m and with an incident ultrasonic wave of pressure amplitude P_m would have a surface velocity given by $u_m = 2P_m/Z_m$. We can compare this with the actual diaphragm velocity u by defining a gain $G = |u/u_m|$. As noted earlier, the acoustic impedance of the diaphragm is small compared to that of the silicone coupling medium. Consequently we can approximate $Z_t \approx 0$ in the transmission line model; yielding the

$$G = \left[1 + \left(\frac{Z_{silicone}^2}{Z_m^2} - 1\right)\sin^2\left(\frac{2\pi t_{silicone}}{\lambda_{silicone}}\right)\right]$$

where ω is the angular frequency and $Z_{silicone}$, $\lambda_{silicone}$, and $t_{silicone}$ are the acoustic impedance, acoustic wavelength, and thickness of the silicone, respectively. In the present case the silicone is considerably less than an acoustic wavelength in thickness and we predict $G \approx 1$.

Note that good coupling will be obtained independent of the ratio $Z_{silicone}/Z_m$ provided the coupling layer is much less than an acoustic wavelength in thickness and $Z_{silicone} > Z_t$. Use of air as a coupling medium is less desirable because (1) $Z_{air} < Z_t$ except very close to the diaphragm resonant frequency and (2) because the underdamped behavior of the diaphragm in air will lead to degraded pulse response.

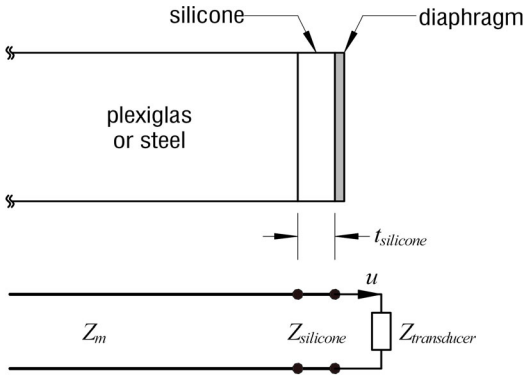

Figure 4. Transmission line model.

V. Ultrasonic Detection

Detection of ultrasonic pulses was demonstrated using plexiglas and metal test specimens. We report here on experiments performed with plexiglas specimens which demonstrate localization of an ultrasonic source using a phased array and flaw detection.

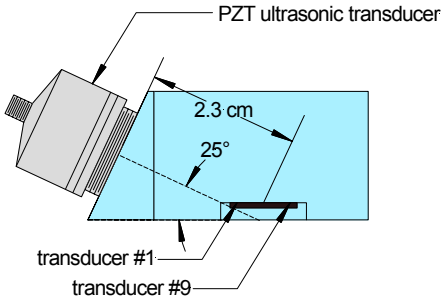

Figure 5. Plexiglas specimen used for testing of the ultrasonic transducer arrays.

Localization experiments were conducted using a plexiglas test specimen arranged for off-axis illumination of the detector array (Fig. 5). A Krautkramer USPC-2100 was used to drive a 3.5 MHz Krautkramer MSW-QC transducer with short pulses. The detectors were biased with 100 V DC and the detected signal was averaged and recorded using a HP 54601A oscilloscope.

In a capacitive transducer the signal current is given by

$$i_{sig} = C_0 \frac{dv}{dt} + v \frac{dC}{dt} \approx V_{DC} \frac{\varepsilon_0 S^*}{g^2} u$$

where u is the velocity of the top plate of the diaphragm, V_{DC} the DC bias voltage, S^* the detector effective area, and g is the gap between top and bottom electrodes.

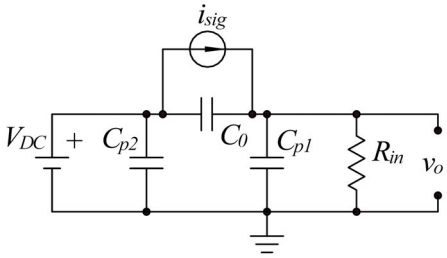

Figure 6. Test circuit.

Figure 6 illustrates the measurement circuit where C_0 models the capacitance of the detector and i_{sig} represents the signal current resulting from the ultrasonic excitation. It is important to note that the magnitude of the observed signal is substantially reduced by stray capacitances C_{p1} and C_{p2} associated with parasitics in our detector design, cable capacitance, and oscilloscope input capacitance.

The measured signals are shown in Fig. 7 for seven of the nine detectors in the array. (One of the nine detectors was not operational and one failed in the course of experiments). Detector #1 was closest to the source (left side of the chip in Fig. 6) and #9 was farthest away. As expected, we observe increasing delay moving from #1 to #9. Note that stray electrical coupling from the exciting pulse causes the small signal at $t = 1$ μsec.

The delay between adjacent transducers is given by $\tau = (d/c) \cdot \cos\theta$ where d is the spacing between transducers and θ is the angle between the emitting transducer and the chip surface.

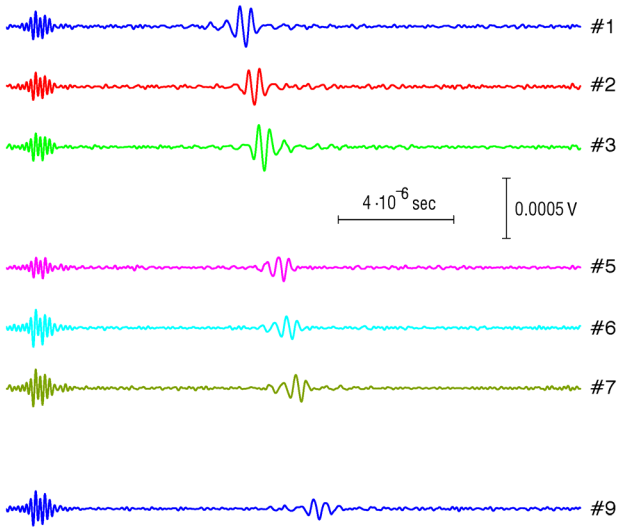

Figure 7. Received pulses with off-axis source.

In order to determine the source location, we plot

$$V(t,\tau) = \sum_n v_n(t - n \cdot \tau)$$

where $v_n(t)$ is the signal from the nth transducer and τ is the delay. This results in a summed signal which depends on the delay time τ. These summed signals are plotted in Figure 8. We observe that all transducer signals add coherently to give the largest summed signal for $\tau = 330$ ns. This yields $\theta = 29$ degrees, in reasonable agreement with the prism shape. The delay for the pulse corresponding to the transducer #5 (the center transducer) is approximately 8.7 μs, giving a distance to the source of 2.35 cm, also in excellent agreement with the test specimen shape

Finally, we report the detection of flaws or voids using capacitative diaphragm transducers. Reflected signals from flaws are significantly smaller than those resulting from direct illumination. Consequently the following measurements utilized an additional (gain = 11) amplifier together with other measures intended to reduce the system noise. In these experiments a 3.5 MHz piezoelectric transducer was the source and Gelest Zipcone TR silicone was used for bonding.

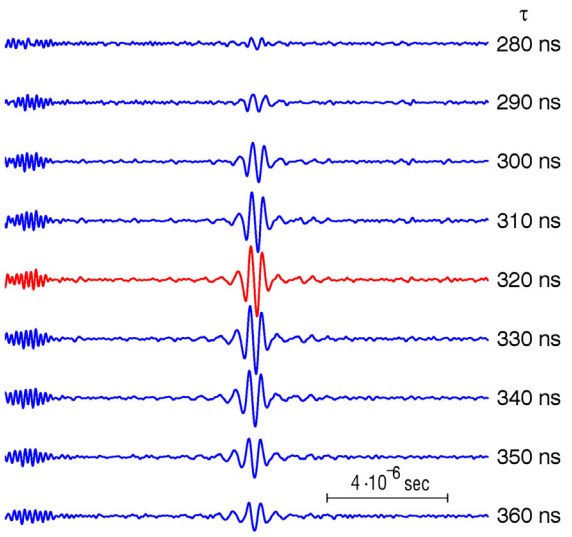

Figure 8. Sum of delayed signals as a function of the delay time τ. A maximum amplitude is obtained when all signals add coherently at $\tau = 330$ ns.

Figure 9 shows the plexiglas flaw test specimen. Reflecting flaws were introduced by drilling two holes of diameters 0.4 and 1.0 cm with differing depth. In this case the line of detectors forming the array is perpendicular to the drawing; consequently the reflected signals should arrive at all detectors simultaneously.

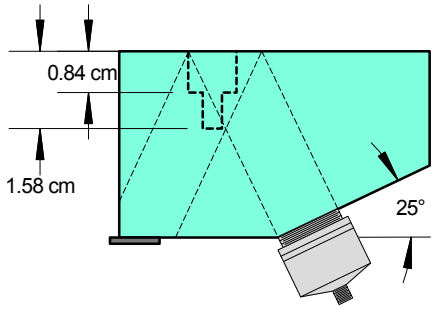

Figure 9. Specimen for demonstration of flaw detection.

The observed rectified signals for four detectors are plotted in Fig. 10. In this case all nine detectors were operational although only four signals are plotted in the figure. Stray electrical coupling causes the first signal at t = 5 μsec, coincident with the exciting pulse. We observe clearly three reflections (small drilled hole, larger drilled hole, and the upper surface of the sample, respectively). The reflections are at 19.0, 23.9, and 30.2 μsec, in good agreement with the values 20.9, 24.2, and 29.5 μsec calculated from the specimen dimensions.

The lower signal levels in the flaw detection experiments are a consequence of the small reflecting area compared to the ultrasonic beam size and also non-optimal beam alignment.

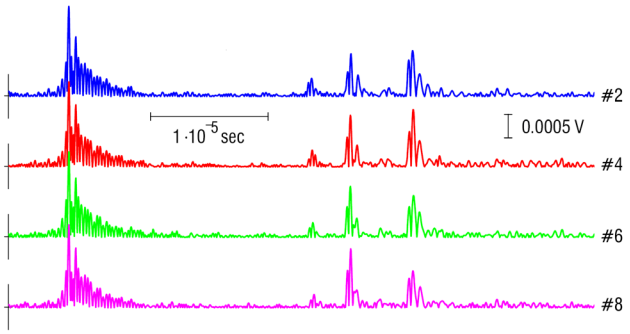

Figure 10. Signal observed by oscilloscope in flaw detection experiment (preamplifier gain = 11).

VI. Conclusions

We have reported the application of MEMS capacitive diaphragm transducers directly coupled to solids. These transducers can potentially be applied to structural monitoring. We have also demonstrated phased-array detection of the location and angular position of a source, and also the detection of flaws in a test specimen.

VII. Acknowledgements

This work has been funded by the Commonwealth of Pennsylvania through the Pennsylvania Infrastructure Technology Alliance program, and by gifts from Krautkramer Inc. The authors would also like to thank R. Rivas for construction of the preamplifier.

VIII. References

[1] "Surface micromachined ultrasound transducers in CMOS technology," P.-C. Eccardt, K. Niederer, T. Scheiter, and C. Hierold, 1996 IEEE Ultrasonics Symposium, pp. 959-962 (1996).

[2] "Micromachined ultrasonic capacitance transducers for immersion applications," A.G. Bashford, D.W. Schindel, D.A. Hutchins, IEEE Transactions on Ultrasonics, Ferroelectrics, and Frequency Control, vol. 45, pp. 367-375 (1998).

[3] "Characterization of one-dimensional capacitive micromachined ultrasonic immersion transducer arrays," X. Jin, I. Ladabaum, F.L. Degertekin, S. Calmes, and B.T. Khuri-Yakub, IEEE Journal of Microelectromechanical Systems, vol. 8, pp. 100-114 (1999).

[4] "Characterization of one-dimensional capacitive micromachined ultrasonic immersion transducer arrays," X. Jin, O. Oralkan, F.L. Degertekin, and B.T. Khuri-Yakub, IEEE Transactions on Ultrasonics, Ferroelectrics, and Frequency Control, vol. 48, pp. 750-760 (2001).

[5] I.J. Oppenheim, A. Jain, and D.W. Greve, (submitted to IEEE Transactions on Ultrasonics, Ferroelectrics, and Frequency Control).